Available online at www.sciencedirect.com
SCIENCE DIRECT
Neural Networks 17 (2004) 647–662
Neural Networks
www.elsevier.com/locate/neunet

2004 Special Issue

A simple cell model with dominating opponent inhibition for robust image processing

Thorsten Hansen[a,*], Heiko Neumann[b]

[a]Department of Psychology, Giessen University, D-35394 Giessen, Germany
[b]Department of Neural Information Processing, Ulm University, D-89069 Ulm, Germany

Received 7 October 2003; revised 1 April 2004; accepted 1 April 2004

Abstract

The extraction of oriented contrast information by cortical simple cells is a fundamental step in early visual processing. The orientation selectivity originates at least partly from the input of lateral geniculate nuclei neurons with properly aligned receptive fields. In the present article, we investigate the feedforward interactions between on- and off-pathways. Based on physiological evidence we propose a push–pull model with dominating opponent inhibition (DOI). We show that the model can account for empirical data on simple cells, such as contrast-invariant orientation tuning, sharpening of orientation tuning with increasing inhibition, and strong response decrements to stimuli with luminance gradient reversal. With identical parameter settings, we apply the model for the processing of synthetic and real world images. We show that the model with DOI can robustly extract oriented contrast information from noisy input. More important, noise is adaptively suppressed, i.e. the model simple cells do not respond to homogeneous regions of different noise levels, while remaining sensitive to small contrast changes. The image processing results reveal a possible functional role of the strong inhibition as observed empirically, namely to adaptively suppress responses to noisy input.

Keywords: Simple cell; Receptive fields; Dominating opponent inhibition

1. Introduction and motivation

At the early stages of visual processing, unoriented contrast signals are extracted by retinal ganglion cells with concentric receptive fields (RFs) and transmitted via the lateral geniculate nuclei (LGN) to the primary visual cortex V1. In V1, simple cells exist which have elongated RFs and a distinct orientation preference. The origin of this orientation selectivity is a field of intense research and controversy debate (see Shapley, Hawken, & Ringach, 2003 for a recent review). It is now widely agreed that tuned feedforward input from LGN neurons with properly aligned RFs (Reid & Alonso, 1995) and cortical inhibition (Borg-Graham, Monier, & Frégnac, 1998; Monier, Chavane, Baudot, Graham, & Fregnac, 2003) are important factors.

The classical proposal by Hubel and Wiesel (1968) was based on feedforward input alone. In their model, simple cell on-subfields receive excitatory input from LGN on-cells, and off-subfields receive excitatory input from LGN off-cells. Based on physiological studies (Ferster, 1988) this basic model has been extended such that each subfield also receives inhibitory input from the opponent pathway. This push–pull model of direct excitation and opponent inhibition assumes an equal weighting of excitatory and inhibitory input. However, a number of empirical studies show that simple cells receive strong inhibitory input which can overwhelm excitatory input. Evidence comes from both extracellular (Heggelund, 1981; Palmer & Davis, 1981) and intracellular recordings (Borg-Graham et al., 1998; Hirsch, Alonso, Reid, & Martinez, 1998). Based on this evidence we propose a scheme of dominating opponent inhibition (DOI) using a stronger weighting of the inhibitory input from the opponent pathway. To generate the final simple cell responses, a non-linear simple cell model using a multiplicative combination of simple cell subfields (MCSCS) is employed (Neumann, Pessoa, & Hansen, 1999).

The model is evaluated in two different respects: simulation of empirical data and processing of images.

* Corresponding author.
E-mail addresses: thorsten.hansen@psychol.uni-giessen.de (T. Hansen), hneumann@neuro.informatik.uni-ulm.de (H. Neumann).

0893-6080/$ - see front matter © 2004 Elsevier Ltd. All rights reserved.
doi:10.1016/j.neunet.2004.04.002

In a first set of simulations we show that the proposed model is consistent with a number of physiological findings on simple cells. In particular, the model can reproduce the physiological data of simple cell responses to luminance gradient reversal (Hammond & MacKay, 1983), where a large decrease of activity occurs if small patches of opposite contrast polarity are added to an optimal bar stimulus. The model also exhibits contrast-invariant orientation tuning (Sclar & Freeman, 1982), where DOI leads to a sharpening of the tuning curves. Having verified the biological relevance of the model by simulating a number of empirical data, we next use the model with identical parameter settings for the processing of noisy synthetic and real world images. The results show that the robustness of the simple cell responses increases for the model with DOI. More important, noise is adaptively suppressed, i.e. the model simple cells do not respond to noisy homogeneous regions, irrespectively of the amount of noise. We have further shown by numerical evaluation that the simple cells with DOI remain sensitive even to small contrasts at edge locations.

This article is organized as follows. In Section 2, the simple cell model together with the proposed mechanism of DOI is formally introduced. Simulation results of physiological data are presented in Section 3. In Section 4, the model is applied for the processing of images, and in Section 5, its response properties to different noise levels and small contrast changes are numerically evaluated. Section 6 concludes the article.

2. The model

In this section a formal description of the model is given. The model consists of a hierarchical organization of two main processing stages, namely the extraction of contrast signals, followed by a simple cell circuit. In all equations, capital Roman letters denote the 2D maps of activity distributions at the various stages and Greek letters denote positively valued model parameters.

2.1. Contrast signals

Contrast signals are generated from the initial luminance distribution of the input stimulus. Contrast signals occur at luminance differences and are intended to model responses of LGN cells. The model equations defining the first processing stage, as detailed in the following, summarize the initial visual processing by the retina and the LGN.

To model contrast signals, the initial luminance distribution is first processed by a center–surround mechanism similar to retinal ganglion cells. Center and surround responses are modeled separately by filtering the initial luminance distribution I with isotropic Gaussians of different standard deviations (SDs) $\sigma_c = 1$ and $\sigma_s = 3$

$$I_c = I * G_{\sigma_c}, \qquad I_s = I * G_{\sigma_s},$$

where $*$ is the spatial convolution operator. The Gaussians are sampled within a 3σ interval, resulting in a filter mask of size 7×7 for the center and 19×19 for the surround ($3\sigma \times 2 + 1$). Input stimuli are normalized to the range [0,1], and the Gaussian filters are normalized such that they integrate to unity.

Center and surround responses provide the input to a shunting mechanism (Furman, 1965; Grossberg, 1970; Hodgkin, 1964). Shunting mechanisms yield a bounded activity and cause a compression of high amplitude activity following the Weber–Fechner law (Fechner, 1889; Weber, 1846):

$$\partial_t X = -\alpha X + (\beta - X)\text{net}^+ - (\gamma + X)\text{net}^-.$$

In the above equation, $\alpha = 0.5$ is the activity decay rate and $\beta = 1$, $\gamma = 0.1$ denote the upper and lower bound of the activity, which is bounded in the interval $[-\gamma, \beta]$.

The shunting equation is assumed to quickly reach steady-state and is solved at equilibrium. The equilibrium solution is given for $\partial_t X = 0$ and can be written as a function X of two input variables, an excitatory contribution net^+ and an inhibitory contribution net^- :

$$X(\text{net}^+, \text{net}^-) = \frac{\beta\text{net}^+ - \gamma\text{net}^-}{\alpha + \text{net}^+ + \text{net}^-}. \tag{1}$$

The shunting interaction is modeled for two domains, namely on and off contrast signals. For the on domain, the excitatory input net^+ is provided by the center filtered input I_c, whereas the inhibitory input net^- is provided by the surround filtered input I_s. The reverse holds true for the off domain. Using the equilibrium function $X(\text{net}^+, \text{net}^-)$, on and off contrast signals X_{on} and X_{off} are thus modeled as

$$X_{on} = X(I_c, I_s), \qquad X_{off} = X(I_s, I_c). \tag{2}$$

These shunting contrast signals exhibit non-zero response to homogeneous regions. As detailed by Neumann (1996), shunting contrast signals can be segregated into a pure contrast signal without any activity to homogeneous regions (i.e. a signal with 'zero DC level') and a luminance signal given by a low-pass filtered copy of the input activity. Following Neumann (1996), zero DC level contrast signals K_{on} and K_{off} result from mutual inhibition of opposite domains

$$K_{on} = [X_{on} - X_{off}]^+, \qquad K_{off} = [X_{off} - X_{on}]^+, \tag{3}$$

where $[x]^+ := \max\{x, 0\}$ denotes half-wave-rectification. The contrast signals K_{on} and K_{off} model LGN responses and provide the input to the next processing stage. To sum up, LGN responses are modeled as rectified non-linear filtering of the input luminance distribution.

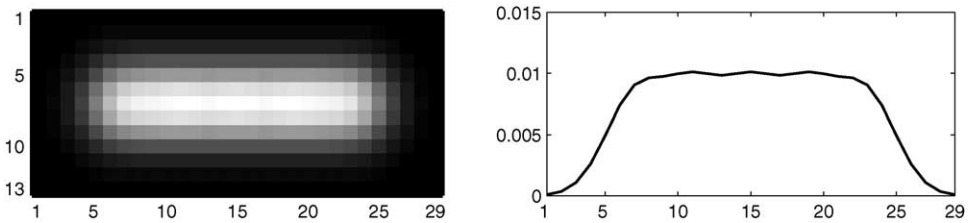

Fig. 1. Left: Filter mask for a simple cell subfield of orientation 0°. Right: The corresponding horizontal cross-section taken at the center of the mask.

2.2. Simple cells

The next processing stage deals with simple cells, which are modeled for $O_{\max} = 8$ discrete orientations $\theta = 0, 22.5, 45, \ldots, 157.5°$ and for two opposite contrast polarities, namely light–dark and dark–light. Light–dark and dark–light simple cells are obtained by sampling the subfield activity with an offset of three pixels orthogonal to the axis of orientation of the simple cell: A light–dark cell has an on-subfield with an offset to the left and an off-subfield with an offset to the right. For a dark–light simple cell, left and right offsets are interchanged. In Section 2.2.1 we detail the modeling of simple cell subfield by the new mechanism of DOI.

2.2.1. Simple cell subfields with dominating opponent inhibition

A simple cell has two adjacent subfields, an on-subfield sensitive to light increments and an off-subfield sensitive to light decrements. Simple cell subfields are defined by elongated, oriented weighting functions G_θ. The weighting function G_θ is modeled with five isotropic Gaussians with SD $\sigma = 2$, which are properly aligned along the preferred axis of orientation θ and spaced within a distance of 2 SDs. A sample weighting function for $\theta = 0°$ is depicted in Fig. 1. The modeling of the weighting function for the simple cell subfields results in a plateau-like RF which is $29/19 \approx 1.5$ times larger than the RF of the on and off cells. Generally, for N Gaussians with a SD σ, spaced within a distance of 2 SD's, the width of the filter mask is given by $2 \times 3\sigma + 1$ and the length of the filter mask is given by $(N-1)2\sigma + 2 \times 3\sigma + 1$. For the parameters chosen $(N = 5, \sigma = 2)$ this results in an aspect ratio (length/width) for the simple cell subfield of $29/13 = 2.23$ (see Fig. 1, left). Alternatively, measuring the subfield aspect ratio by fitting an anisotropic Gaussian results in a larger aspect ratio of $7.5/2 = 3.75$. Physiological studies differ in the aspect ratio measured for simple cells. Aspect ratios of 5 and larger have been reported (Gardner, Anzai, Ohzawa, & Freeman, 1999; Jones & Palmer, 1987a,b), while others have found considerably smaller aspect ratios with a mean of 1.7 (Pei, Vidyasagar, Volgushev, & Creutzfeldt, 1994). Recently, Alonso, Usrey, and Reid (2001) found aspect ratios ranging from 1.17 to 5.45, with a mean of 2.5 ± 0.8 (mean $\pm$ SD). Similar values have been obtained by Kara, Pezaris, Yurgenson, and Reid (2002), who found a mean aspect ratio of 2.7 ± 0.8. We conclude that the aspect ratio of our filter is in reasonable agreement with the physiological data.

Before integration, contrast activity of different polarity competes at each spatial location. Input activation for both on and off subfields R_{on} and R_{off} with a preferred orientation θ is computed by convolution of the weighted difference of unoriented LGN responses K_{on} and K_{off} with the subfield mask G_θ of the same orientation preference:

$$R_{\text{on},\theta} = [(K_{\text{on}} - \xi K_{\text{off}}) * G_\theta]^+,$$
$$R_{\text{off},\theta} = [(K_{\text{off}} - \xi K_{\text{on}}) * G_\theta]^+. \tag{4}$$

A sketch of the interaction scheme which defines the subfields is given in Fig. 2. The case of equally weighted on and off inputs occurs for $\xi = 1$. The newly proposed scheme of dominating opponent inhibition (DOI) introduces a weighting parameter $\xi > 1$ which scales up the opponent contribution. This introduces a 'one against many' situation, where, e.g. an on-subfield only receives input if the contribution of the on-channel K_{on} is ξ times larger than the contribution of the opponent off-channel K_{off}. The subfield interaction with DOI is a special case of the push–pull models (Ferster, 1988; Palmer & Davis, 1981; Tolhurst

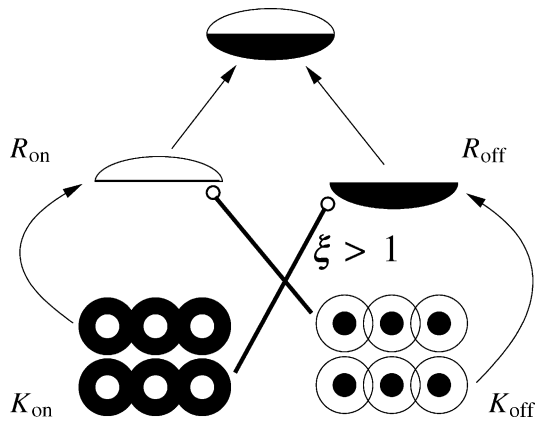

Fig. 2. Simple cell model with DOI. An on-subfield R_{on} receives excitatory input from properly aligned LGN on-cells K_{on} and inhibitory input from LGN off cells K_{off}. The scheme of dominating opponent inhibition proposes a stronger weighting of the inhibitory input with $\xi > 1$, as indicated by the thicker lines. The reverse wiring pattern exists for the off subfields R_{off}. Arrows denote excitatory input, circles at the end of lines denote inhibitory input. For clearness of display, subfields are drawn separated.

& Dean, 1990). Conventionally, the pull is provided by simple cells with RFs of opposite contrast polarity (Ferster & Miller, 2000; Troyer, Krukowski, Priebe, & Miller, 1998). The new scheme of DOI, on the other hand, assumes that inhibitory input is provided by cells which are not orientation selective and have a circular RF organization. Recently, a possible neural substrate of DOI has been reported, namely complex smooth cells in layer 4 which are inhibitory and untuned for orientation (Hirsch, Martinez, Pillai, Alonso, Wang, & Sommer, 2003).

The mechanism may also be interpreted in terms of voting, where excitatory and inhibitory inputs represent voting in favor or against a decision, i.e. whether the subfield responds or not. For balanced inhibition, a simple majority of 50% votes in favor results in a subfield response. For dominating inhibition, a majority greater than 50% of votes in favor are required to cause a response. More precisely, for a weighting of the opponent inhibition with $\xi > 1$, the excitatory drive has to comprise a fraction of $\xi/(\xi + 1)$ of the total input to drive the cell. In terms of voting, this means that for setting, say, $\xi = 2$, a 2/3 majority is required to result in a response of the subfield.

DOI processing has important effects on the behavior of the model. It is the key feature for simulating data in a physiological study on luminance gradient reversal (Section 3.1), and it makes the model more robust to noise (Sections 4 and 5). As stated above, DOI relies on strong inhibition. The assumption of strong inhibitory input to a simple cell that can overwhelm excitatory contributions is supported by many physiological studies. Evidence comes from both extracellular (Heggelund, 1981; Palmer & Davis, 1981) and intracellular recordings (Borg-Graham et al., 1998; Ferster, 1988; Hirsch et al., 1998).

2.2.2. Non-linear simple cell circuit

On and off subfields interact via a disinhibition circuit that boosts activities for spatially juxtaposed on and off contrast configurations (Neumann et al., 1999). Such juxtaposed on and off contrasts occur at step edges, thus the simple cell model exhibits significantly higher responses for this configuration than for shallow luminance gradients, for example.

The resulting simple cell activity consists of a linear and a non-linear, i.e. multiplicative, term

$$\tilde{S} = \frac{\alpha_S(R_{on} + R_{off}) + 2\beta_S(R_{on}R_{off})}{\alpha_S\gamma_S + \beta_S\gamma_S(R_{on} + R_{off})}. \quad (5)$$

The parameters are set to $\alpha_S = 1.0$, $\beta_S = 10,000.0$, and $\gamma_S = 0.01$. Their specific choice is not critical as long as the linear components scaled by α_S and γ_S are small compared to the non-linear component scaled by β_S. For the normalized input image with values in the range [0,1], the parameterization of the model results in values of the subfield activity R_{on} and R_{off} which are considerably below one. To guarantee that multiplication of these values actually leads to an increase of activity compared to the linear addition result in the strong weighting of the non-linear part in Eq. (5). Further details of the non-linear simple cell circuit can be found in Appendix A.

In some of the simulations, the proposed non-linear integration of simple cell subfields is compared to a basic linear integration where subfield responses R_{on} and R_{off} are simply added. For the linear subfield interaction, Eq. (5) is replaced by

$$\tilde{S}_{lin} = R_{on} + R_{off}. \quad (6)$$

Here and in the following we refer to the model with a linear combination of simple cell subfields as 'quasi-linear', since this model contains non-linearities at the pre-processing stages.

To sum up, the present simple cell model comprises two mechanisms with complementary functionality. DOI serves to suppress undesired spurious activity to noisy inputs, while the non-linear simple cell circuit sharpens and amplifies desired responses to edges.

2.3. Complex cells

Complex cell responses are insensitive to contrast polarity and are modeled by pooling responses of simple cells with opposite contrast polarity

$$C_\theta = S_{ld,\theta} + S_{dl,\theta}. \quad (7)$$

Pooled complex cell responses C_{pool} result from summing complex cell responses for all orientations

$$C_{pool} = \sum_\theta C_\theta. \quad (8)$$

Pooled complex cells responses are used in Sections 4 and 5 to visualize the responses of the whole model within a single image.

3. Simulations of physiological data

In order to demonstrate the physiological plausibility and relevance of the proposed model, basic properties of simple cells found in vivo are simulated. In particular, we simulate a study of Hammond and MacKay (1983), to show that DOI processing can account for both classical linear response up to saturation as well as strong depression effects as measured by Hammond and MacKay. Further, we determined orientation tuning curves for the model simple cells to study the effect of DOI on the tuning widths. The simulations show a sharpening of orientation tuning with increasing inhibition, in accordance with physiological findings (Shapley et al., 2003). The values of the model parameters are as described in Section 2 and are the same in all simulations, except for the orientation tuning simulations in Section 3.2 where 16 orientations are used to allow for a sufficiently fine resolution of orientation space.

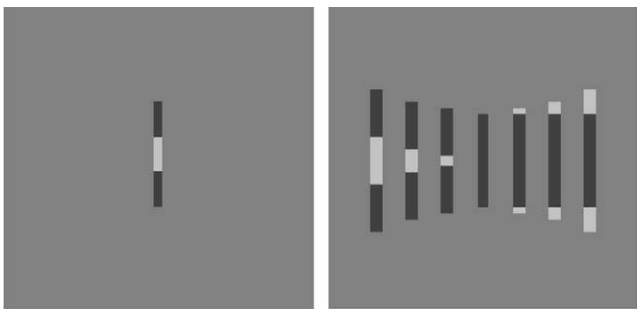

Fig. 3. Left: Example of stimulus used. Right: A set of stimuli for a fixed length of the dark bar.

3.1. Hammond and Mackay study

In this section we simulate a study of Hammond and MacKay (1983), who investigated the response of simple cells in cat to optimally oriented bars. This study is challenging for any model of simple cells because it shows classical effects like linear contrast summation up to saturation and strong, possibly non-linear, suppressive effects.

In their study, Hammond and MacKay recorded simple cell responses to three types of bar stimuli: dark bars, dark bars with light segments added in the middle (DLD) and dark bars with light segments added at both ends (LDL).

Fig. 3 depicts the single stimulus used and a sample of the whole stimulus set. A main result of their work is shown in Fig. 4. Probing a simple cells without end-inhibition with bars of different lengths results in a linear response up to saturation ('length-summation curve').

When light segments are added to the dark bars (DLD and LDL), the average response decrement is much larger than predicted from linear contrast summation. Linear summation would suggest that the slopes of the length-summation curve and of the LDL and DLD curves are the same.

Our model predicts that simple cell responses as observed by Hammond and MacKay can be generated on the basis of the proposed DOI scheme. Results are shown in Fig. 4 (right). The same model parameters as for the processing of images in Section 4 are employed. The declining slopes of the curves for both DLD and LDL stimuli are much steeper than the ascending slope of the length-summation curve, as reported by Hammond and MacKay. In summary, a good qualitative fit with the physiological data is obtained. Note that for the non-dominant case, i.e. setting the DOI parameter $\xi = 1$, no strong suppression occurs, but the responses for LDL and DLD bar stimuli lie on the dotted line as predicted by linear contrast summation. To rule out effects of the non-linear simple cell circuit, the circuit is replaced by a linear combination of simple cell subfields, where subfield responses are simply added (Eq. (6)). For this model variant with DOI, the results obtained are qualitatively the same.

3.2. Orientation tuning

The most prominent RF property of simple cells is their orientation selectivity. One can plot orientation tuning curves of simple cells by measuring the mean firing rate of a simple cell for stimulus items of different orientations. Orientation tuning curves of simple cells have a Gaussian shape which peaks at the preferred orientation. The half-width at half-height (HWHH) of the orientation tuning

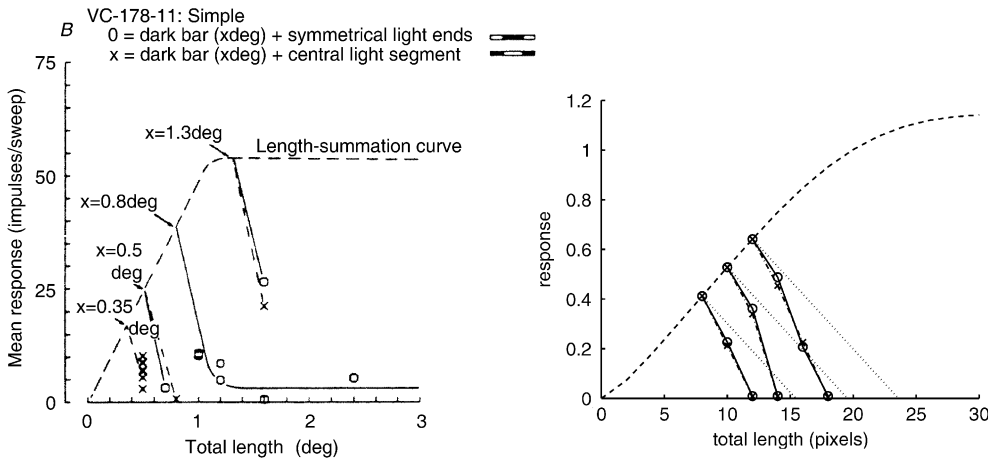

Fig. 4. Physiological recording and simulation results of simple cell responses to a dark bar alone (length-summation curve, dashed) and a dark bar with added segments of opposite contrast polarity. Segments of opposite contrast polarity are added either at the ends (LDL bars, data points marked 'o', solid line) or centrally (DLD bars, data points marked 'x', dashed line). The abscissae denote total bar length (dark bar plus light segments). Left: Results of physiological recordings by Hammond and MacKay (1983). Response curves to LDL and DLD bars are extrapolated to the response for the dark bar alone (as indicated by arrows pointing to the length-summation curve). Curves are free-hand approximations to the data points. Data reprinted with permission of the publisher. Right: Simulation result. For comparison, predictions by linear contrast summation (dotted) are shown in the plot of the simulated data. Both the physiological study and the simulations show a strong response decrement when a light segment is added to the dark bar. The decrement for segments of opposite contrast polarity is much stronger than the corresponding response increment for a segment of the same contrast polarity (compare slopes of length-summation curves with slopes of curves for LDL and DLD bars).

curves is used as a measure which characterizes the sharpness of orientation tuning.

In this section we simulate orientation tuning curves to study the effects of DOI and the subsequent linear vs. non-linear combination of simple cell subfields on the orientation selectivity of model simple cells. To determine orientation tuning curves, we probe the circuit with sinusoidal grating stimuli of different contrasts. For computational convenience, rather than using grating stimuli of different orientations, we determined orientation tuning curves from simple cells responses with a number of $O_{\max} = 16$ different orientations at the same fixed location (Troyer et al., 1998). The location is chosen which results in maximal response for a linear light–dark simple cell and is kept fixed for all model variants studied. We parameterize the simple cell model with $O_{\max} = 16$ different orientation instead of $O_{\max} = 8$ (Section 2) to allow for a sufficiently fine resolution of orientation space. The number of $O_{\max} = 16$ orientations results in sampling of orientation space of $180°/16 = 11.25°$. To rule out that the tuning curves depend on the sampling of stimulus orientations we have rerun the simulations with $O_{\max} = 32$ orientations. For all cases shown in the following, the HWHHs differed by less than 1°.

In a first study, we compare the effect of DOI on orientation tuning curves for the linear and the combination of simple cell subfields (Fig. 5). As a basic result, for both the linear and the non-linear combination of simple cell subfields, DOI, i.e. increasing the inhibition at the level of LGN cells, results in a sharper orientation tuning. Note that DOI has only small effects on the response magnitude of the optimally tuned cell. Further, the orientation tuning curves of the linear and the non-linear combination of subfields exhibit two general differences. First, the orientation tuning curves sharply fall off for the non-linear combination and more smoothly roll off for the linear combination. Second, the width of the curves is smaller for the non-linear than for the linear combination. To sum up, both DOI and non-linear processing have the effect of decreasing the width of the tuning curves, with non-linear processing additionally sharpens the shape of the curves. Consequently, the highest selectivity is obtained for the model with the, MCSCS together with DOI.

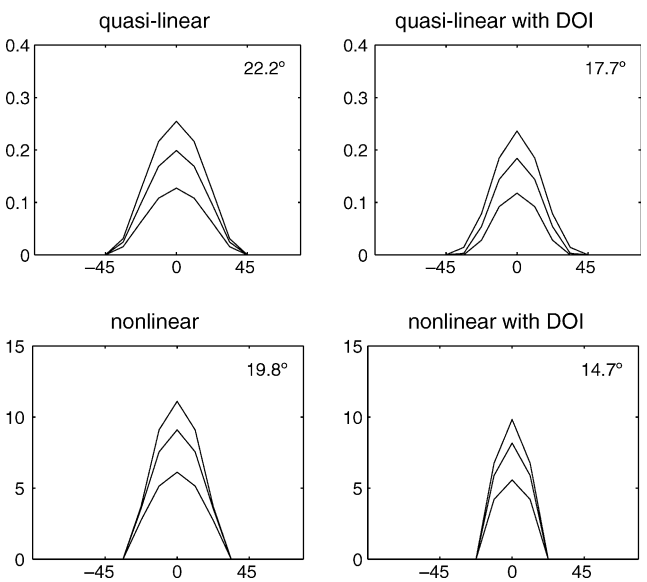

Fig. 5. Orientation tuning curves for models with linear and non-linear combination of subfields, both with and without DOI. The abscissa denotes orientation in degree, the ordinate denotes the simple cell response at a fixed spatial location. The three curves in each plot correspond to different contrast levels, namely 0.8, 0.5 and 0.25 (top to bottom). Top right inset denotes mean HWHH. The orientation tuning curves show contrast-invariant orientation tuning for all four models and a sharpening of orientation tuning by DOI.

Physiological recordings of simple cells tuning curves show that the tuning curves remains constant, even when the contrast of the stimulus is changed (Sclar & Freeman, 1982; Skottun, Bradley, Sclar, Ohzawa, & Freeman, 1987). All model variants show this contrast-invariant orientation tuning. As pointed out by Ferster and Miller (2000), this property is difficult to explain in a simple feedforward model, because the responses of both retinal ganglion cells and LGN cells strongly depend on stimulus contrast (Cheng, Chino, Smith, Hamamoto, & Yoshida, 1995; Troy & Enroth-Cugell, 1993).

The width of orientation tuning of simple cells in vivo exhibits a certain variation. The HWHH between orientation tuning curves in monkey varies between 5 and 50°, with a most frequent tuning of 20° (Schiller, Finlay, & Volman, 1976). More recently, Carandini and Ferster (2000) have found an average HWHH for the spike responses of simple cells of 23°. The values obtained for the models are thus in good agreement with the physiological experiments. Because of the high aspect ratio of the filter used to model the simple cell subfield, the HWHH of the quasi-linear model also falls within the physiological range.

Shapley et al. (2003) summarize physiological data which show a direct correlation between the amount of

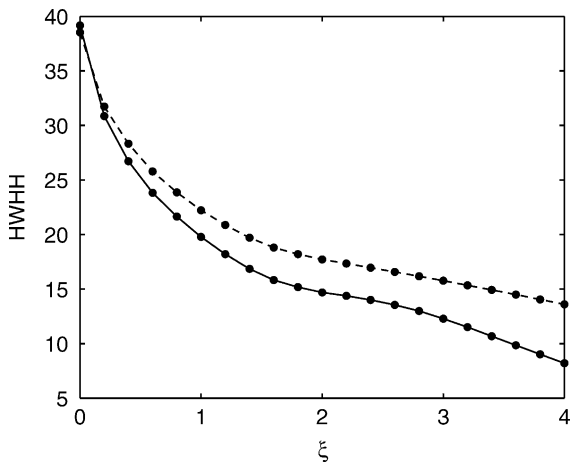

Fig. 6. Sharpening or orientation tuning with increasing inhibition. Both models with either a linear (upper curve, dashed) or a non-linear combination of simple cell subfields (lower curve, solid), show a sharpening of orientation tuning, i.e. a monotonically decrease in HWHH with increasing amount of inhibition by increasing the DOI parameter ξ. Simulated data points are marked with dots.

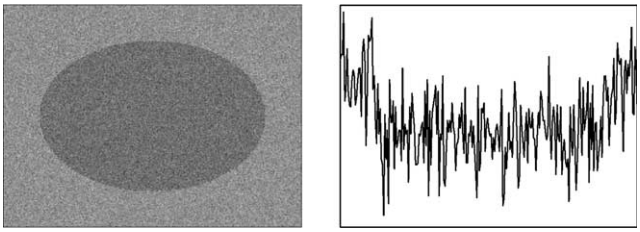

Fig. 7. Noisy ellipse (left) and corresponding horizontal cross-section (right) taken at the center of the image. The size of the ellipse image is 253 × 189 pixels.

inhibition a neuron receives and its orientation selectivity. In a second study, we determine HWHHs of orientation tuning curves for different amounts of inhibition by varying the DOI parameter ξ in the range [0,4]. As above, simulations are carried out for two model variants with a linear or non-linear combination of simple cell subfields. The results are shown in Fig. 6. For both models, increasing the amount of inhibition results in an increasingly sharper orientation tuning. Compared to the linear combination of simple cell subfields, the non-linear combination has an overall higher orientation selectivity. To sum up, the model shows the direct correlation between the amount of inhibition a neuron receives and its orientation selectivity, as observed physiologically (Shapley et al., 2003).

4. Processing of images

In this section, we show the performance of the model on synthetic and on natural images. The values of the model parameters are as described in Section 2 and are the same in all simulations. In the simulations we compare the new mechanism of DOI (setting $\xi = 2$) to a model with a linear combination of subfields and to the non-linear model without DOI ($\xi = 1$). Recall that for the linear combination of subfields the subfield responses are simply added to replace the non-linear interactions of Eq. (5). As noted above, we refer to this model as 'quasi-linear', since it contains non-linearities at the pre-processing stages. The model with the linear combination of subfields approximates filtering with a first order Gaussian derivative (Neumann et al., 1999). The edge images show pooled complex cell response (Eq. (8)), dark values indicate high responses.

4.1. Synthetic images

In the first study we employ a synthetic image of a dark ellipse on a lighter background, corrupted with 50% additive Gaussian noise. Fig. 7 shows the input image together with a horizontal cross-section taken at the center of the image.

For this image, four results are generated by combining two interactions at the subfield level (standard and DOI) with two combinations of the subfields (linear and non-linear). The simulation results are shown in Fig. 8. All models show pronounced responses at the edge locations, but only the non-linear models have a unimodal response to an edge. Moreover, the results show that the models with DOI are considerably less sensitive to noise. The simulation results for this image exemplify the complementary properties of DOI and of the non-linear simple cell circuit: DOI serves to suppress noisy inputs, while the non-linear interaction of MCSCS sharpens the responses to edges.

The edge doubling observed for the quasi-linear model occurs when the half-wave rectified input from LGN on and off cells is processed by model simple cells with adjacent on and off subfields. More precisely, the edge doubling results from simple cells which have the same orientation as the edge, but reversed contrast-polarity. Consider a light–dark edge which generates adjacent on and off contrast responses. The light–dark simple cell with matching RF subfields responds strongest at the edge location. However, also the dark–light simple cell with reversed RF subfields responds at

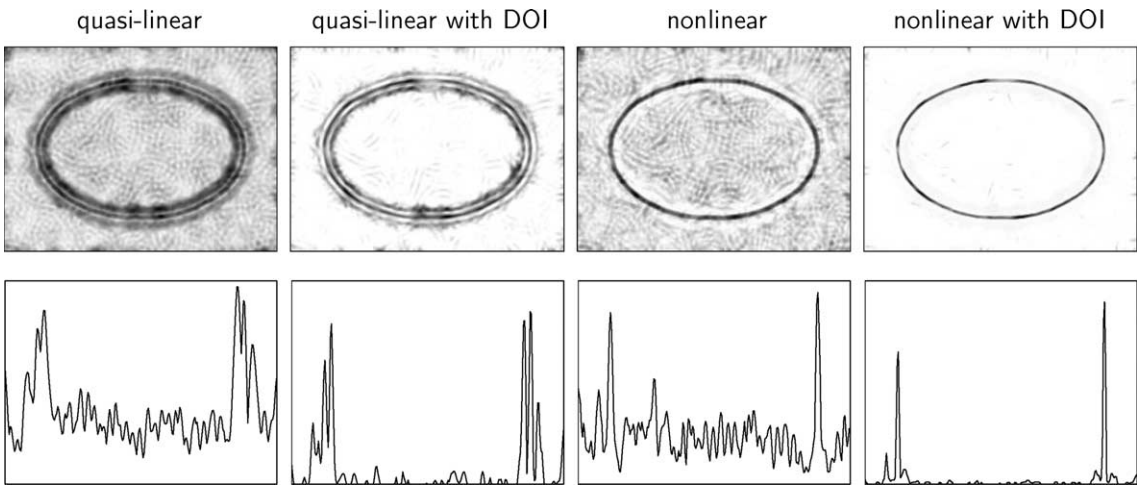

Fig. 8. Top row: Simulation results for the image of a noisy ellipse. Bottom row: The corresponding horizontal cross-sections taken at the center of the images. The size of the images is 253 × 189 pixels.

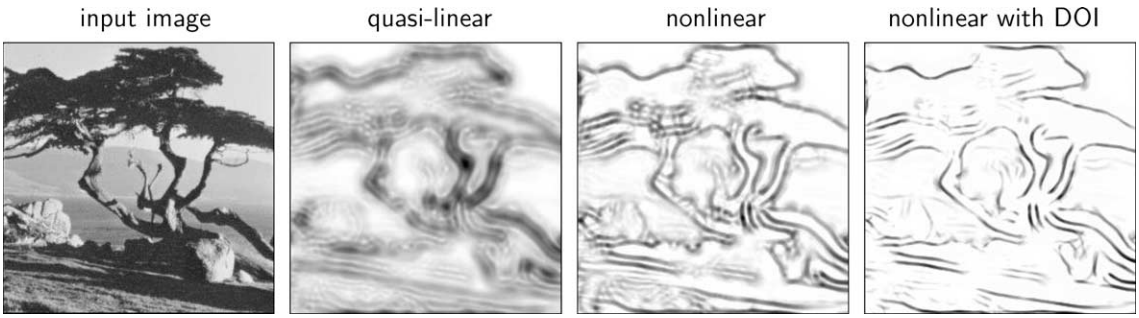

Fig. 9. Natural image of a tree and simulation results. The size of the images is 255 × 256 pixels.

a location left to edge, due to the integration of on responses by the on-subfield, and also right to the edge, due to the integration of off responses by the off-subfield. Lateral inhibition cannot remove these double responses: while the undesired side responses are inhibited by the stronger central response, at the same time the central desired responses would be inhibited by the two side responses. Also, inhibition between simple cell of opposite contrast-polarity, as has been used in a previous version of our model, still results in double responses for the linear model. Note that a linear filtering of the raw input luminances without the intermediate stage of half-wave-rectified LGN responses would not result in edge doubling. The edge-doubling is thus a property of our particular model, not a fundamental problem confronting linear processing schemes.

4.2. Natural images

A further challenge to the model is posed by processing of natural images. In the first simulation we use an image of a tree which is shown together with the simulation results in Fig. 9. For the DOI processing, responses to the lawn are largely suppressed, while responses to the contour of the tree and to the shadow are enhanced. We also employ an image of a 3D laboratory scene as input image (Fig. 10). Here, the contours of the cube are sharper and the spurious responses at the floor vanish for DOI processing.

In two further simulations, we employ images from a set used in an evaluation study of edge detection algorithms (Heath, Sarkar, Sanocki, & Bowyer, 1997). We use a larger scale to show the simulation results to compensate for the approximately doubled image size compared to the previously shown images.

For the traffic cone, the DOI processing results in sharp, pronounced responses to the shape outline of the cone and the car, while spurious responses to the leaves are successfully suppressed. Similar results are obtained for the image of a golf cart, where the edges of the cart are reliably detected, while responses to small noisy structures such as the lawn and the leaves are suppressed by DOI (Figs. 11 and 12).

In some of the simulation results, the DOI processing seems to suppress also responses to low contrast edges. This effect is studied in detail in Section 5.1. It turns out that the small responses are also retained for DOI processing, but their visibility is reduced due to the rendering of the simulation results.

5. Evaluation of DOI properties

In Section 4 we have qualitatively shown that DOI allows for the robust processing of images. In this section we further clarify the properties of DOI in a series of numerical evaluations.

To motivate the simulations in this section it is instructive to consider the DOI equation, Eq. (4), in more detail. Using Eq. (3) and the equality $[x]^+ - [-x]^+ = x$, we

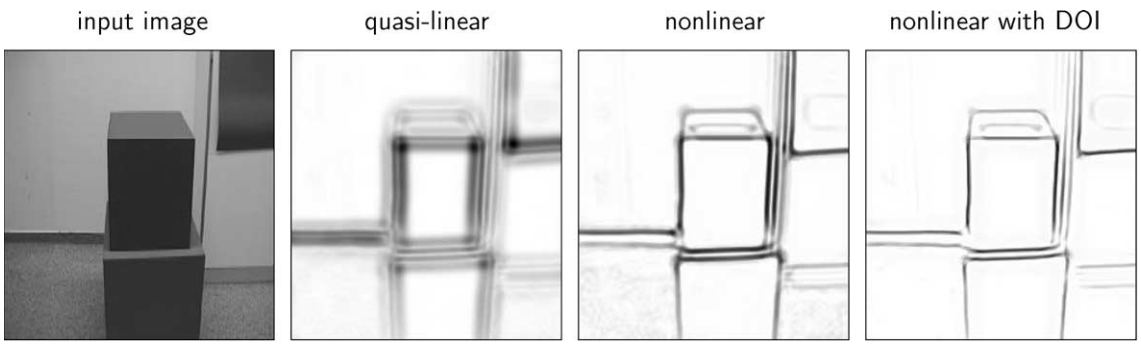

Fig. 10. Image of a laboratory scene and simulation results. The size of the images is 230 × 246 pixels.

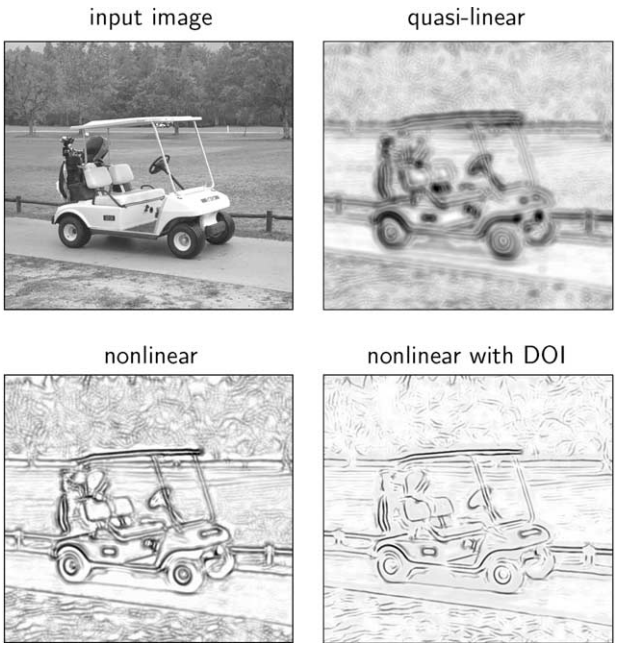

Fig. 11. Golf cart image and simulation results. The edge images are gamma corrected with $\gamma = 0.6$ because of the high contrast variations in the image. The size of the images is 548×509 pixels.

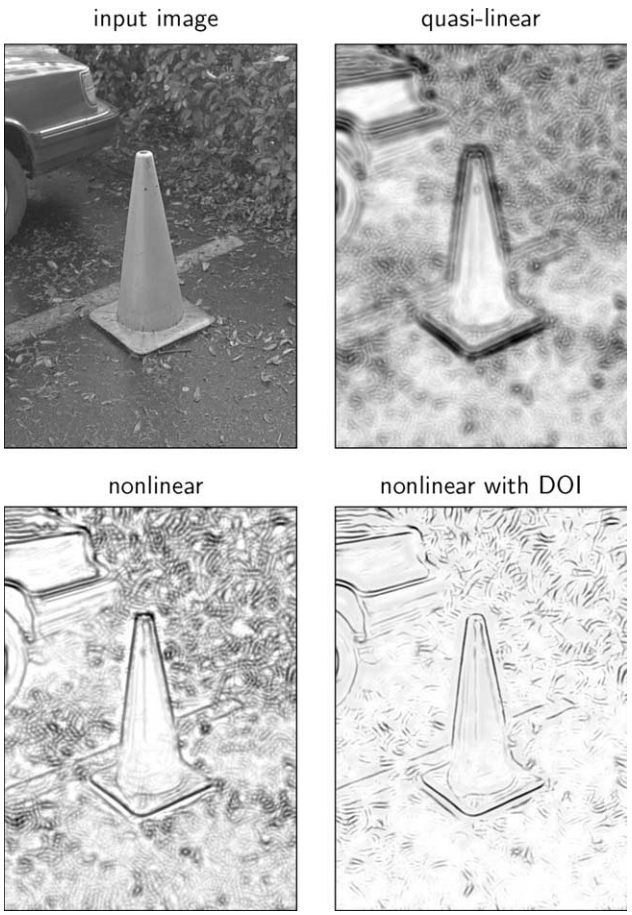

Fig. 12. Traffic cone image and simulation results. The edge images are gamma corrected with $\gamma = 0.6$ because of the high contrast variations in the image. The size of the images is 437×604 pixels.

can rewrite Eq. (4) as follows:

$$\begin{aligned} R_{\text{on},\theta} &= [(K_{\text{on}} - \xi K_{\text{off}}) * G_\theta]^+ \\ &= [(K_{\text{on}} - K_{\text{off}}) * G_\theta - (\xi - 1)K_{\text{off}} * G_\theta]^+ \\ &= [(X_{\text{on}} - X_{\text{off}}) * G_\theta - \underbrace{(\xi - 1)K_{\text{off}} * G_\theta}_{\text{dynamic threshold}}]^+. \end{aligned} \tag{9}$$

This shows that DOI interaction introduces a dynamic threshold that is proportional to ξ and depends on the strength of the signal in the opponent pathway.

With respect to this adaptive threshold it needs to be clarified to what extent desired responses to contrast changes might be suppressed by DOI interaction. This question is addressed in a first set of simulations where we evaluate the response of DOI to small contrast changes. We show that the model with DOI remains sensitive even to small contrast changes in the presence of noise. In a second set of simulations we investigate the choice of the DOI parameter ξ to meet two conflicting demands as goods as possible, namely the suppression of noise and the responsiveness to contrast changes. The response to different noise levels further shows an important feature of DOI, namely the adaptive suppression of noise.

5.1. Response to small contrasts

In this section, the effect of DOI on the processing of small contrast changes is addressed, to examine whether DOI has an undesired suppressive effect on contrast responses. To study this question the response to small contrast changes in the presence of high level noise is evaluated for three simple cells models, namely a model with a linear combination of subfields, and a non-linear combination of subfields without and with DOI.

For the simulations a synthetic test image of alternating on–off and off–on vertical step edges of increasing contrast is employed. The on–off contrasts vary from 0.01 to 0.1 in steps of 0.01 and are centered around a mean luminance level of 0.5. For each on–off contrast, the image contains an individual subimage of size 128×256 pixels, resulting in a total stimulus size of 1280×256 pixels. The image together with a horizontal cross-section is depicted in Fig. 13.

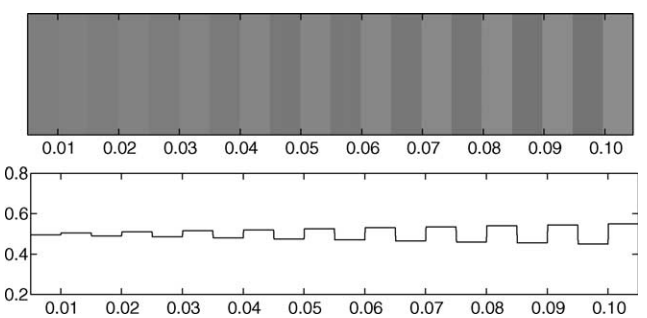

Fig. 13. Top row: Test image for small contrast responses. Bottom row: The corresponding horizontal cross-sections. The values at the abscissa denote the contrast of the step edge at this position.

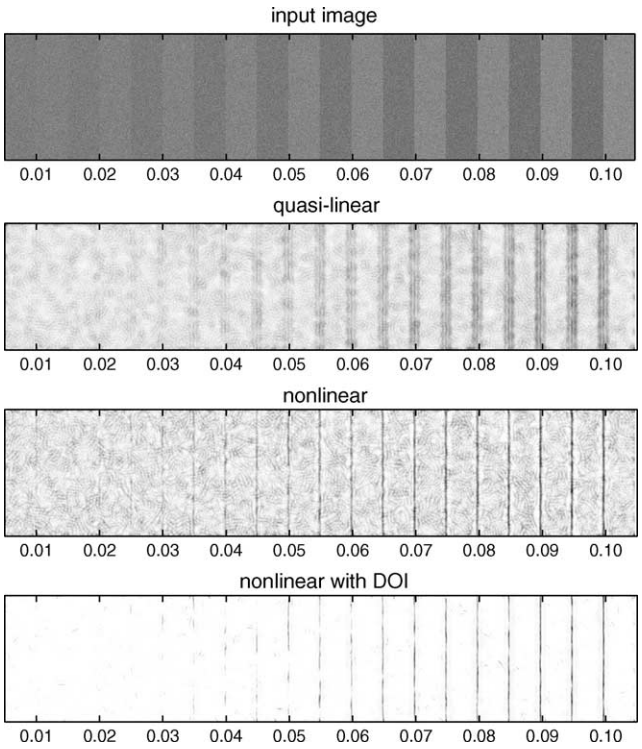

Fig. 14. Test image corrupted with noise of SD 0.05 and corresponding simulation results.

In a pioneering study, the test image is corrupted with Gaussian noise of SD 0.05 which is equivalent to 500% noise for the smallest contrast and 50% for the largest contrast. The input image and the simulation results showing pooled complex cell responses for each of the three simple cell models are depicted in Fig. 14. Most obviously, the result produced by the model with DOI differs from the results produced by the models without DOI in the response to noise. With DOI, responses to noise are absent or at least largely suppressed. At the same time, upon first visual inspection, the model with DOI indeed seems to suppress responses to small contrast. For example, compare the response to the contrasts of 0.04 for the three models. While both models using either a linear or a non-linear combination of simple cell subfields but yield a visible response without DOI, using DOI the response appears fragmented and faint.

To further analyze this behavior, the mean response along each column is computed for the three models (Fig. 15). The plots show that all models yield a mean response above the mean noise level for contrast values of about 0.03 and higher. The reasons why these responses are visible for the two models without DOI but seem to fade for the model with DOI are caused by the properties of the visual display. For each model the resulting image as shown in Fig. 14 is scaled individually, mapping the lowest value to white and the highest to black. Without DOI, the responses to the edges add on a significant noise level, such that, e.g. the mean response to 0.4 contrast has a strength of about 30% of the maximum response, making it fairly visible. For DOI, on the other hand, the noise level is virtually zero, and the mean response to 0.4 contrast is only at about 5% of the maximum response, making it virtually invisible. Thus, the almost vanishing response to noise for the model with DOI renders the response to small contrast less visible, though this response is still present.

Next we determine for each model the contrast level at which the response differs significantly from the response to the noisy background. Therefore, the mean responses and SDs at each dark–light contrast step (signal) are computed and compared to the mean response and SD at the background (noise). Results for the three simple cells models are shown in Fig. 16.

The plots allow to determine the contrast which yields a significant response. A significant response is to be found at contrast locations where the error bars of signal and noise do not overlap. The results show that the amount of contrast, which is necessary to yield a significant response, is the same for all models, in this case 0.05 contrast. Similar results have been obtained for different noise levels. We conclude that the simple cell model with DOI remains sensitive even to small contrast changes, and that any apparent loss of sensitivity can be attributed to the properties of the visual display.

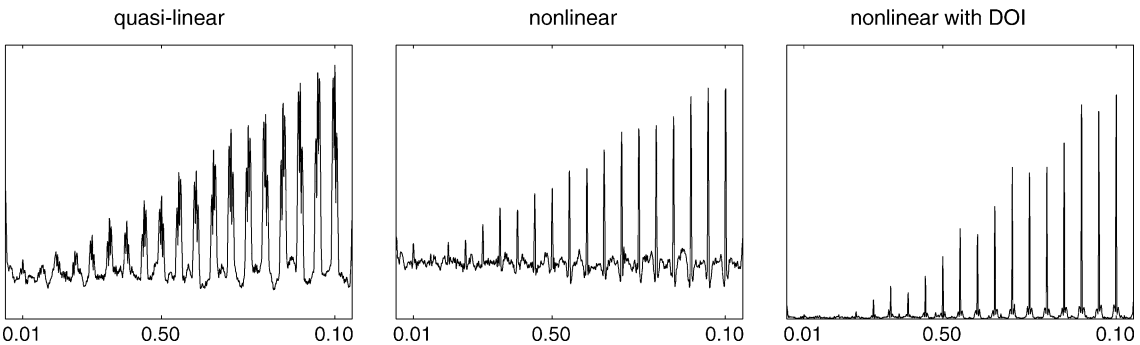

Fig. 15. Column sum of simulation results shown in Fig. 14, using a test image which is corrupted with noise of SD 0.05. The abscissa denotes the contrast of the step edges.

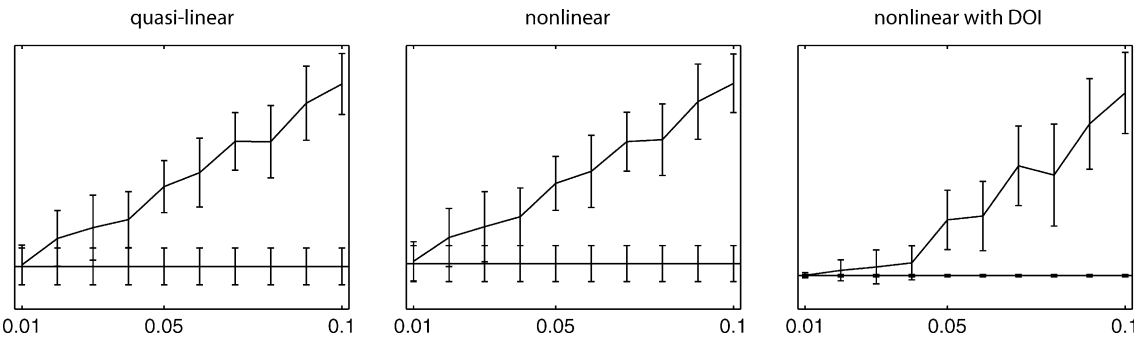

Fig. 16. Mean response at dark–light contrast edges (upper line) compared to mean response at the background (lower horizontal line) for the three models. Error bars denote ±SD. The abscissa denotes the contrast of the step edges. For all three models, a significant response occurs at 0.05 contrast.

5.2. Determination of the DOI parameter and adaptive noise suppression

In this section we investigate the choice of the DOI parameter ξ to meet two conflicting demands as goods as possible, namely the suppression of noise and the responsiveness to contrast changes. We use a step edge which is corrupted with Gaussian noise of different noise levels. Both the response of an optimally oriented subfield and a non-optimally, i.e. orthogonally oriented subfield are simulated for three different noise levels (25, 50 and 80%), and different values of the DOI parameter ξ. Responses are averaged over 100 different realizations for each noise level.

Simulation results are shown in Fig. 17. For the optimal orientation (Fig. 17, left), responses are a lineary decreasing function of ξ, indicating that ξ cannot be chosen arbitrarily large. For the non-optimal orientation (Fig. 17, right), responses decrease non-linearly and are almost zero for $\xi > 2$. Interestingly, this is true for different noise levels, showing that DOI can adaptively suppress noise. 'Adaptive' here refers to the fact that different noise levels (25, 50, and 80%) result in virtually zero response at the non-optimal orientation for $\xi = 2$, i.e. with DOI. Using DOI, the amount of suppression thus adapts to the noise level: the larger the noise, the larger the suppression.

These results provide criteria for the choice of ξ. For a value of $\xi \approx 2$, the non-optimal responses are almost zero, while the optimal responses are still considerably large. Increasing ξ beyond 2 would mostly decrease the optimal responses but not the non-optimal responses, which have already smoothly approached zero. Thus, a value of $\xi = 2$ is chosen for all the simulations of the non-linear model with DOI as presented in Section 3.

6. Discussion and conclusion

6.1. Principle findings

In this article we have proposed a simple cell model with DOI. DOI is integrated into a push–pull interaction defining the simple cell subfield responses. In push–pull interaction, a subfield (e.g. on) receives both excitatory input from the like domain (i.e. on) and inhibitory input from the opposite domain (i.e. off). DOI proposes a stronger weighting of the opponent input, resulting in a more selective response.

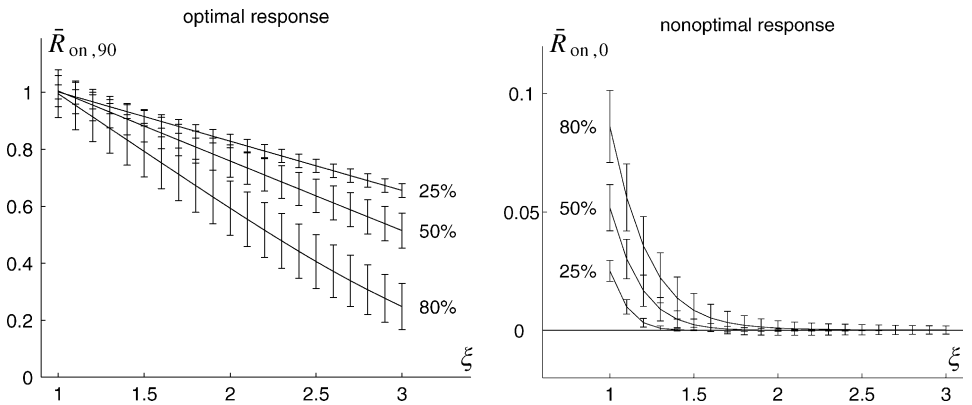

Fig. 17. The mean subfield responses to a noisy step edge, corrupted with 25, 50, and 80% additive Gaussian noise for various values of the DOI parameter ξ. Responses are averaged over 100 different realizations of the respective noise level; error bars denote ±1 SD. Responses are normalized to allow for better comparison. Left: The mean response of an optimally oriented subfield decreases linearly with ξ. Right: The mean response of non-optimally oriented subfield decreases non-linearly with ξ and is almost zero for $\xi = 2$, irrespectively of the amount of noise added. For the non-optimal response (left), we have rescale y-axis to increase the visibility of the plot.

The subfields are combined using a non-linear simple cell model (Neumann et al., 1999).

The proposed model can account for a number of empirical findings. The model reproduces the physiological data of simple cell responses to luminance gradient reversal (Hammond & MacKay, 1983), showing a large decrease of activity if small patches of opposite contrast polarity are added to an optimal bar stimulus. We have further investigated the orientation tuning of model simple cells. The results show that both DOI and MCSCS lead to a sharpening of the orientation tuning. We show that the newly proposed model of simple cells with DOI and MCSCS can generate sharp orientation tuning from simple cell subfields with a physiologically plausible aspect ratio. The model further shows contrast-invariant orientation tuning, an important feature of simple cells in vivo (Ohzawa, Sclar, & Freeman, 1985; Sclar & Freeman, 1982). Next we investigated the correlation between inhibition and the sharpness of orientation tuning. We show that the orientation tuning monotonically increases (i.e. the HWHH decreases) with increasing weighting of the inhibitory input to the simple cell subfield, in accordance with physiological findings (Shapley et al., 2003).

After simulating empirical findings from physiology, the model is used with identical parameter settings to process noisy synthetic and natural images. The results show that the robustness of the response increases for the model with DOI. The model with DOI has a lower probability of responding to noise, while the sensitivity to salient edges is preserved. Finally, we conduct a detailed numerical evaluation to clarify the role of DOI. We particularly focus on the strength of the DOI parameter and the response to small contrasts. We determine an optimal parameter value of $\xi = 2$ which is used in all simulations, and show that the DOI mechanism remains sensitive to small contrasts. The numerical evaluation further shows a unique property of DOI, namely the *adaptive* suppression of noise. The adaptive suppression results in equally good suppression for noise of different levels, as shown in Fig. 17. Adaptive suppression is generated in our model since the amount of suppression, i.e. the activity in the opponent channel, scales with the noise level.

Finally, we presented a numerical evaluation of the DOI properties to address two important questions. First, one might ask whether the good suppression of noise for the DOI model might be accompanied by the undesired feature of suppressing responses to small contrast changes. Here it is shown that a model with DOI does not lead to a gross suppression of small contrast changes, but instead remains sensitive to small contrast variations. However, the results also show that the model with DOI does not outperform the other models with respect to contrast sensitivity, i.e. the lower response to noise does not cause a significantly better response at lower contrast compared to the other models. Second, one might ask what are the advantages of DOI compared to a simple threshold. The advantages can be seen when the model is probed with images of different noise levels. Without DOI, different noise levels lead to an increase of undesired responses to homogeneous regions and at orientations orthogonal to the edge. Most important, this increase is proportional to the noise level: the larger the noise, the stronger are the undesired responses. A threshold then has to be carefully determined by an additional mechanism, depending on the noise level. Further, consider an image with regions of different noise levels. Here, a global threshold cannot distinguish between signal and noise, and elaborated methods of local threshold determination needs to be applied. With DOI, on the other hand, undesired responses to homogeneous regions or at non-optimal orientations orthogonal to an edge are strongly suppressed. Most important, suppression is equally effective irrespectively of the noise level. This is the adaptive noise suppression property of DOI: as noise increases, the amount of suppression adapts to the noise level, such that for different noise levels undesired responses are virtually zero. With DOI, the adaptive thresholding necessary to handle noise of different levels does not require an extra mechanism, but instead is achieved implicitly by an elegant, biologically motivated interaction.

6.2. Use of shunting inhibition vs. linear DoG

The present model uses non-linear shunting interactions for the first processing stage. Shunting interaction has a number of useful properties such as automatic gain-control and response normalization which results in bounded activity and contrast-sensitivity depending on the overall luminance level, following the Weber–Fechner law (Grossberg, 1970). In contrast to the non-linear shunting interaction, a linear interaction using a difference of Gaussians (DoG) model is frequently used. The shunting equations result in a scaled DoG normalized by a sum of Gaussians and comprises of more general form of the basic DoG model (Mingolla, Ross, & Grossberg, 1999; Neumann, 1996). We have rerun a number of simulations with a basic DoG filter instead of the shunting interactions. Replacing the shunting interactions with a similar DoG filter essentially preserves all basic properties of the proposed simple cell model. The proposed mechanisms of DOI and MCSCS are thus robust against changes in the pre-processing stage.

6.3. Comparison with dominating inhibition as used in the model by Troyer et al. (1998)

Dominating inhibition is also used in a detailed physiological model by Troyer et al. (1998) to explain contrast-invariant orientation tuning of simple cells. In contrast to our non-linear model, Troyer et al. (1998) use linear Gabor filters to model simple cells. Strong 'anti-phase' inhibition occurs between Gabor filters of phase shift 180°, i.e. opposite contrast polarity, while we employ inhibition between isotropic on and off responses.

One crucial difference between the model by Troyer et al. (1998) and our model is thus the generation of contrast-

invariant orientation tuning. In our model, contrast-invariant orientation tuning arises also with a basic linear model using balanced inhibition, whether Troyer et al. (1998) proposes stronger inhibition than excitation. Thus, contrary to Troyer et al. (1998), our model predicts that simple cells which receive balanced excitation and inhibition also show contrast-invariant orientation tuning. Provided that intra-cortical recurrent interaction may also play a significant role in generating contrast-invariant orientation tuning, we suggest a different functional role of DOI. On the basis of our findings we suggest that the visual system mainly uses DOI to robustly extract oriented contrast features in noisy environments.

Another important difference between the model by Troyer et al. (1998) and our model is the orientation selectivity of the inhibition. Whereas the model by Troyer et al. (1998) proposes orientation selective inhibition from cells with respond in a contrast-dependent manner, DOI in our model is untuned for orientation. Recently, two populations of inhibitory cells have been found in layer 4, namely orientation selective simple cells and unoriented smooth complex cells (Hirsch et al., 2003). Thus, both kinds of inhibition are supported by biological data. The first version of our model included a stage of oriented inhibition following the non-linear combination of simple cell subfields. At this stage of opposite contrast polarity inhibition, a simple cells receives inhibitory input from a simple cell of same orientation, but opposite contrast polarity. Eliminating this stage did not influence the proposed model in a significant way. Recent work suggests that orientation selective suppression accounts for the dynamical reduction of orientation bandwidth (Ringach, Hawken, & Shapley, 2003). The precise functional roles of the two kinds of inhibition remains to be clarified by future research.

6.4. Relation of the findings by Hammond and MacKay (1983) to studies showing excitatory influence of flanking bars

A number of physiological studies have found excitatory influences of flanking bars on-cell responses (Gilbert, 1992; Gilbert & Wiesel, 1990; Kapadia, Ito, Gilbert, & Westheimer, 1995). The bar stimuli used in these experiments are reminiscent of the DLD and LDL stimuli used by Hammond and MacKay (1983), who found strong inhibitory rather than excitatory influences. However, the stimuli used in both kinds of experiments differ in two important aspects. First, the stimuli used by, e.g. Kapadia, Westheimer, and Gilbert (2000), extend well beyond the classical RF and reveal excitatory long-range influences. On the contrary, Hammond and MacKay (1983) reported strong suppression even when small segments are added and the whole stimulus is confined to the classical RF. Second, the stimuli used in the long-range experiments consist of bars split into a central part and two adjacent flankers, where the gap between the individual parts of the bar has the same contrast as the background. On the contrary, Hammond and MacKay (1983) added segments of opposite contrast polarity to the bars, which was crucial to generate strong suppression. Merely breaking a bar into segments and filling the gaps with the background luminance caused no more reduction than predictable from the effective reduction in bar length (Hammond & MacKay, 1983). Contextual long-range interactions have motivated numerous models for contour and feature linking (Grossberg & Mingolla, 1985; Li, 1998), cortico-cortical interactions for boundary processing (Neumann & Sepp, 1999), pre-attentive texture segmentation (Li, 1999), perceptual grouping and object-based attention (Grossberg & Raizada, 2000), or junction detection (Hansen & Neumann, 2004). A review of computational models can be found in Neumann and Mingolla (2004) or Hansen (2003). In contrast to these models, the present article focuses on suppressive and facilitatory feed-forward interactions within the classical RF.

6.5. Response of white noise stimuli

A number of physiological studies use white noise variations as stimuli and then determine the response properties and RF profiles of cells by reverse correlation techniques (Marmarelis & Marmarelis, 1978; Marmarelis & Naka, 1972). This method has been applied in various studies to determine the spatio-temporal response properties of cells (Cottaris & Valois, 1998; Ringach, 2002; Ringach, Hawken, & Shapley, 1997). The reverse correlation method using white noise stimuli would also work with DOI occurring in vivo, since as the noise pattern resembles the signal, DOI has been shown to be as selective as a mechanisms without DOI (Section 5.1).

6.6. Model extensions: grouping, multiple scales, complementary processing streams

The edge maps produced by the proposed model are clean and sharp, but occasionally contain some gaps. These gaps can be successfully handled by later stages involving contextual grouping mechanisms. Without DOI, the non-zero input to later stages might be caused by a contrast change or, alternatively, by noisy fluctuations within the signal. With DOI, on the other hand, a non-zero response is a strong indication of a contrast change in the original signal. Consequently, with DOI, grouping of local edge information is not plagued by noisy responses but instead integrates only the signal responses. A full evaluation of the benefits of DOI for subsequent stages of grouping mechanisms is an interesting question for future research.

The need to extract image structures such as edges at multiple scales has a long tradition in computer vision and biological modeling (Marr, 1982; Marr & Hildreth, 1980; Witkin, 1983). A more recent discussion can be found in Lindeberg (1994). The present model operates on single

scale but can be naturally extended to the processing at multiple scales by increasing the SDs of the Gaussians that define the model RFs. We have shown in earlier work that the non-linear simple cell circuit has a scale selective property by boosting activity at the appropriate scale that corresponds to the underlying image structure (Neumann et al., 1999). In the present paper, we use a single scale to focus on the contributions of the new mechanism of DOI.

The present model deals with the processing of boundary information. Surface information such as shading and textures can be processed by a parallel surface system, which interacts by filling-in processes with the boundary system (Cohen & Grossberg, 1984; Grossberg, Mingolla, & Ross, 1997). A review can be found in Neumann and Mingolla (2003).

7. Conclusion

Overall, we have presented a biologically motivated simple cell model which incorporates two mechanisms: DOI in a push–pull network, and MCSCS. The model can account for a number of basic empirical findings, such as linear contrast-summation up to saturation and contrast-invariant orientation tuning, as well as for more challenging data such as strong suppression by segments of opposite contrast polarity, sharp orientation tuning using simple cell subfields with a moderate aspect ratio of 2.23, and increasing orientation selectivity with increasing inhibition. Application of this model for the processing of images leads to robust extraction of contrast information by adaptive suppression of noise. This in turn allows to hypothesize a functional role for the dominant inhibition as observed experimentally, showing the fruitful cross-fertilization between biological modeling and more technically oriented applications.

Acknowledgements

We acknowledge the insightful comments and criticisms of two anonymous reviewers whose suggestions helped to improve the article considerably.

Appendix A. Details of the non-linear simple cell circuit

The purpose of the non-linear simple cell circuit is to generate sharp responses at edges. Edges are characterized by spatially juxtaposed on and off contrast responses. To generate a sharp response, the desired circuitry thus has to amplify responses if both subfields are simultaneously active, similar to a soft AND gate. The circuit that realizes this property is motivated computationally and is not supposed to have a direct neurophysiological counterpart.

The various parts of the non-linear simple cell circuitry and their different computational roles are explained below. A more detailed description and motivation of the non-linear simple cell circuit is given in Neumann et al. (1999).

The circuit which defines the multiplicative combination of simple cell subfields (MCSCS) comprises three intermediate steps, namely $S^{(1)}$, $S^{(2)}$, and $\tilde{S}$ (Fig. A1). The basic circuitry is given by the excitatory $R_{\text{on/off}} \rightarrow S^{(2)}_{\text{on/off}} \rightarrow \tilde{S}$ connections, which define the excitatory input to the simple cell from its two subfields R_{on} and R_{off}. A circuit having only this basic connection would results in a simple cell that linearly sums its input. To make the circuit more selective for juxtaposed on and off contrasts, additional connections are introduced. The on-channel path $R_{\text{on}} \rightarrow S^{(1)}_{\text{on}} \multimap S^{(2)}_{\text{on}}$ implements a self-normalization by inhibition of $S^{(2)}_{\text{on}}$, which prevents arbitrarily large activity of the cell. The same holds true for the off-channel. The key connections of the model are the cross-channel inhibitory connections $R_{\text{on}} \multimap S^{(1)}_{\text{off}}$ and $R_{\text{off}} \multimap S^{(1)}_{\text{on}}$. By disinhibition, i.e. inhibiting the inhibition of $S^{(1)}$, the simple cell response is non-linearly amplified if both subfields are active simultaneously.

The first two steps are modeled using inhibitory shunting equations. The steady-state solutions for the on-channel read

$$S^{(1)}_{\text{on}} = \frac{R_{\text{on}}}{\alpha_{\text{S}} + \beta_{\text{S}} R_{\text{off}}}, \qquad S^{(2)}_{\text{on}} = \frac{R_{\text{on}}}{\gamma_{\text{S}} + \delta_{\text{S}} S^{(1)}_{\text{on}}}.$$

The corresponding equations for the off-channel are obtained by interchanging on and off. Variables occur for all discrete orientations. The index θ is omitted to simplify

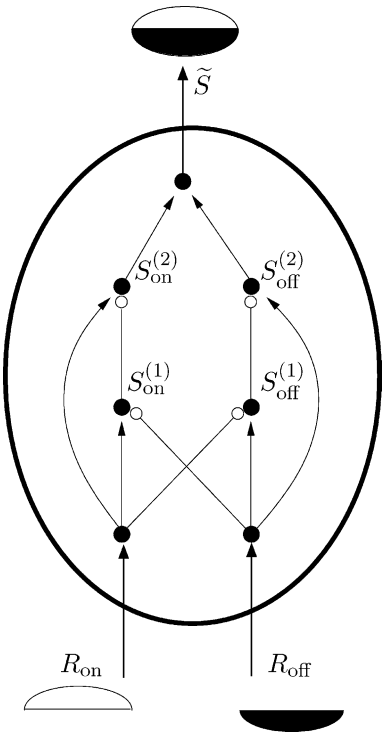

Fig. A1. Sketch of the simple cell circuit with the non-linear, multiplicative combination of simple cell subfields (MCSCS). Arrows denote excitatory input, circles at the end of lines denote inhibitory input.

notation. The activity of the third step $\tilde{S}$ results from pooling the contributions of the on and off-channel

$$\tilde{S} = S^{(2)}_{\text{on}} + S^{(2)}_{\text{off}}.$$

Combining these equations and assuming a symmetric relation between the two channels by setting $\delta_S = \beta_S \gamma_S$ yields a more concise equation. The resulting simple cell activity consists of a linear and a non-linear, i.e. multiplicative, term

$$\tilde{S} = \frac{\alpha_S(R_{\text{on}} + R_{\text{off}}) + 2\beta_S(R_{\text{on}}R_{\text{off}})}{\alpha_S\gamma_S + \beta_S\gamma_S(R_{\text{on}} + R_{\text{off}})}.$$

The parameters are set to $\alpha_S = 1.0$, $\beta_S = 10,000.0$, and $\gamma_S = 0.01$. Their specific choice is not critical as long as the linear components scaled by α_S and γ_S are small compared to the non-linear component scaled by β_S.

References

Alonso, J. M., Usrey, W. M., & Reid, R. C. (2001). Rules of connectivity between geniculate cells and simple cells in cat primary visual cortex. *The Journal of Neuroscience*, *21*(11), 4002–4015.

Borg-Graham, L. J., Monier, C., & Frégnac, Y. (1998). Visual input evokes transient and strong shunting inhibition in visual cortical neurons. *Nature*, *393*, 369–373.

Carandini, M., & Ferster, D. (2000). Orientation tuning of membrane potential and firing rate responses in cat primary visual cortex. *The Journal of Neuroscience*, *20*, 470–484.

Cheng, H., Chino, Y. M., Smith, E. L., III, Hamamoto, J., & Yoshida, K. (1995). Transfer characteristics of lateral geniculate nucleus X neurons in the cat: Effects of spatial frequency and contrast. *Journal of Neurophysiology*, *74*(6), 2548–2557.

Cohen, M., & Grossberg, S. (1984). Neural dynamics of brightness perception: Features, boundaries, diffusion, and resonance. *Perception and Psychophysics*, *36*, 428–456.

Cottaris, N. P., & De Valois, R. L. (1998). Temporal dynamics of chromatic tuning in macaque primary visual cortex. *Nature*, *395*(6705), 896–900.

Fechner, G. T. (1889). *Elemente der Psychophysik*. Leipzig: Breitkopf & Härtel.

Ferster, D. (1988). Spatially opponent excitation and inhibition in simple cells of the cat visual cortex. *The Journal of Neuroscience*, *8*(4), 1172–1180.

Ferster, D., & Miller, K. D. (2000). Neural mechanisms of orientation selectivity in visual cortex. *Annual Review of Neuroscience*, *23*, 441–471.

Furman, G. (1965). Comparison of models for subtractive and shunting lateral-inhibition in receptor-neuron fields. *Kybernetik*, *2*, 257–274.

Gardner, J. L., Anzai, A., Ohzawa, I., & Freeman, R. D. (1999). Linear and nonlinear contributions to orientation tuning of simple cells in the cat's striate cortex. *Visual Neuroscience*, *16*(6), 1115–1121.

Gilbert, C. D. (1992). Horizontal integration and cortical dynamics. *Neuron*, *9*(1), 1–13.

Gilbert, C. D., & Wiesel, T. N. (1990). The influence of contextual stimuli on the orientation selectivity of cells in primary visual cortex of the cat. *Vision Research*, *30*(11), 1689–1701.

Grossberg, S. (1970). Neural pattern discrimination. *Journal of Theoretical Biology*, *27*, 291–337.

Grossberg, S., & Mingolla, E. (1985). Neural dynamics of perceptual grouping: Textures, boundaries, and emergent segmentation. *Perception and Psychophysics*, *38*, 141–171.

Grossberg, S., Mingolla, E., & Ross, W. D. (1997). Visual brain and visual perception: How does the cortex do perceptual grouping? *Trends in Neurosciences*, *20*(3), 106–111.

Grossberg, S., & Raizada, R. D. S (2000). Contrast-sensitive perceptual grouping and object-based attention in the laminar circuits of primary visual cortex. *Vision Research*, *40*(10), 1413–1432.

Hammond, P., & MacKay, D. (1983). Influence of luminance gradient reversal on simple cells in feline striate cortex. *The Journal of Physiology*, *337*, 69–87.

Hansen, T (2003). *A neural model of early vision: Contrast, contours, corners and surfaces*. Doctoral dissertation, Ulm University, Faculty of Computer Science, Department of Neural Information Processing. Available on-line: http://vts.uni-ulm.de/query/longview.meta.asp?document_id = 3022.

Hansen, T., & Neumann, H. (2004). Neural mechanisms for the robust detection of junctions. *Neural Computation*, *16*(5), 1013–1037.

Heath, M. D., Sarkar, S., Sanocki, T., & Bowyer, K. W. (1997). A robust visual method for assessing the relative performance of edge-detection algorithms. *IEEE Transactions of Pattern Analysis and Machine Intelligence*, *19*(12), 1338–1359.

Heggelund, P. (1981). Receptive field organization of simple cells in cat striate cortex. *Experimental Brain Research*, *42*, 89–98.

Hirsch, J. A., Alonso, J. M., Reid, R. C., & Martinez, L. M. (1998). Synaptic integration in striate cortical simple cells. *The Journal of Neuroscience*, *18*(22), 9517–9528.

Hirsch, J. A., Martinez, L. M., Pillai, C., Alonso, J. M., Wang, Q., & Sommer, F. T. (2003). Functionally distinct inhibitory neurons at the first stage of visual cortical processing. *Nature Neuroscience*, *6*(12), 1300–1308.

Hodgkin, A. L. (1964). *The conduction of nervous impulses*. Liverpool: Liverpool University Press.

Hubel, D. H., & Wiesel, T. N. (1968). Receptive fields and functional architecture of monkey striate cortex. *The Journal of Physiology*, *195*, 215–243.

Jones, J. P., & Palmer, L. A. (1987a). The two-dimensional spatial structure of simple receptive fields in cat striate cortex. *Journal of Neurophysiology*, *58*(6), 1187–1211.

Jones, J. P., & Palmer, L. A. (1987b). An evaluation of the two-dimensional Gabor filter model of simple receptive fields in cat striate cortex. *Journal of Neurophysiology*, *58*(6), 1233–1258.

Kapadia, M. K., Ito, M., Gilbert, C. D., & Westheimer, G. (1995). Improvement in visual sensitivity by changes in local context: Parallel studies in human observers and in V1 of alert monkeys. *Neuron*, *15*(4), 843–856.

Kapadia, M. K., Westheimer, G., & Gilbert, C. D. (2000). Spatial distribution of contextual interactions in primary visual cortex and in visual perception. *Journal of Neurophysiology*, *84*(4), 2048–2062.

Kara, P., Pezaris, J. S., Yurgenson, S., & Reid, R. C. (2002). The spatial receptive field of thalamic inputs to single cortical simple cells revealed by the interaction of visual and electrical stimulation. *Proceedings of National Academy of Sciences of the United States of America*, *99*(25), 16261–16266.

Li, Z. (1998). A neural model of contour integration in the primary visual cortex. *Neural Computation*, *10*(4), 903–940.

Li, Z. (1999). Pre-attentive segmentation in the primary visual cortex. *Spatial Vision*, *13*, 25–50.

Lindeberg, T. (1994). *Scale-space theory in computer vision*. Boston: Kluwer.

Marmarelis, P. Z., & Marmarelis, V. Z. (1978). *Analysis of physiological systems*. New York: Plenum Press.

Marmarelis, P. Z., & Naka, K. (1972). White-noise analysis of a neuron chain: An application of the Wiener theory. *Science*, *175*(27), 1276–1278.

Marr, D. (1982). *Vision*. San Francisco, CA: W.H. Freeman & Co..

Marr, D., & Hildreth, E. (1980). Theory of edge detection. *Proceedings of the Royal Society of London (B)*, *207*, 187–217.

Mingolla, E., Ross, W. D., & Grossberg, S. (1999). A neural network for enhancing boundaries and surfaces in synthetic aperture radar images. *Neural Networks*, *12*, 499–511.

Monier, C., Chavane, F., Baudot, P., Graham, L. J., & Fregnac, Y. (2003). Orientation and direction selectivity of synaptic inputs in visual cortical neurons: A diversity of combinations produces spike tuning. *Neuron*, *37*(4), 663–680.

Neumann, H. (1996). Mechanisms of neural architecture for visual contrast and brightness perception. *Neural Networks*, *9*(6), 921–936.

Neumann, H., & Mingolla, E. (2003). Contour and surface perception. In M. Arbib (Ed.), *Handbook of brain theory and neural networks* (pp. 271–276). Cambridge, MA: MIT Press.

Neumann, H., & Mingolla, E (2001). Computational neural models of spatial integration and perceptual grouping. In T. F. Shipley, & P. J. Kellman (Eds.), *From fragments to objects: Segmentation and grouping in vision*, Vol. 130 of *Advances in psychology*, chap. 12 (pp. 353–400). Amsterdam: Elsevier.

Neumann, H., Pessoa, L., & Hansen, T. (1999). Interaction of ON and OFF pathways for visual contrast measurement. *Biological Cybernetics*, *81*(5–6), 515–532.

Neumann, H., & Sepp, W. (1999). Recurrent V1–V2 interaction in early visual boundary processing. *Biological Cybernetics*, *81*, 425–444.

Ohzawa, I., Sclar, G., & Freeman, R. D. (1985). Contrast gain control in the cat's visual system. *Journal of Neurophysiology*, *54*(3), 651–667.

Palmer, L. A., & Davis, T. L. (1981). Receptive field structure in cat striate cortex. *Journal of Neurophysiology*, *46*, 260–276.

Pei, X., Vidyasagar, T. R., Volgushev, M., & Creutzfeldt, O. D. (1994). Receptive field analysis and orientation selectivity of postsynaptic potentials of simple cells in cat visual cortex. *The Journal of Neuroscience*, *14*(11 Pt 2), 7130–7140.

Reid, R. C., & Alonso, J. M. (1995). Specifity of monosynaptic connections from thalamus to visual cortex. *Nature*, *378*, 281–284.

Ringach, D. L. (2002). Spatial structure and symmetry of simple-cell receptive fields in macaque primary visual cortex. *The Journal of Neurophysiology*, *88*(1), 455–463.

Ringach, D. L., Hawken, M. J., & Shapley, R. (1997). Dynamics of orientation tuning in macaque primary visual cortex. *Nature*, *387*, 281–284.

Ringach, D. L., Hawken, M. J., & Shapley, R. (2003). Dynamics of orientation tuning in macaque V1: The role of global and tuned suppression. *The Journal of Neurophysiology*, *90*(1), 342–352.

Schiller, P. H., Finlay, B. L., & Volman, S. F. (1976). Quantitative studies of single-cell properties in monkey striate cortex. ii. Orientation specificity and ocular dominance. *The Journal of Neurophysiology*, *39*, 1321–1333.

Sclar, G., & Freeman, R. D. (1982). Orientation selectivity in the cat's striate cortex is invariant with stimulus contrast. *Experimental Brain Research*, *46*(3), 457–461.

Shapley, R., Hawken, M., & Ringach, D. L. (2003). Dynamics of orientation selectivity in the primary visual cortex and the importance of cortical inhibition. *Neuron*, *38*(5), 689–699.

Skottun, B. C., Bradley, A., Sclar, G., Ohzawa, I., & Freeman, R. D. (1987). The effect of contrast on visual orientation and spatial frequency discrimination: A comparison of single cells and behavior. *The Journal of Neurophysiology*, *57*(3), 773–786.

Tolhurst, D. J., & Dean, A. F. (1990). The effects of contrast on the linearity of spatial summation of simple cells in the cat's striate cortex. *Experimental Brain Research*, *79*, 582–588.

Troy, J. B., & Enroth-Cugell, C. (1993). X and Y ganglion cells infor the cat's brain about contrast in the retinal image. *Experimental Brain Research*, *93*, 383–390.

Troyer, T. W., Krukowski, A. E., Priebe, N. J., & Miller, K. D. (1998). Contrast-invariant orientation tuning in cat visual cortex: Thalomocortical input tuning and correlation-based intracortical connectivity. *The Journal of Neuroscience*, *18*(15), 5908–5927.

Weber, E.H (1846). Tastsinn und Gemeingefühl. In R. Wagner (Ed.), *Handwörterbuch der Physiologie*. Reprinted in W. Ostwald (1905), *Klassiker der exakten Wissenschaften*, Vol. 149. Leipzig: Engelmann.

Witkin, A. P. (1983). Scale-space filtering. *In Proceedings of the 8th International Joint Conference on Artificial Intelligence (IJCAI)*, *2*, 1019–1022.